Received 13 February 2018; revised 28 March 2018; accepted May 9 2018. Date of publication 22 May 2018;
date of current version 8 June 2018. The review of this paper was arranged by Editor S. Reggiani.

Digital Object Identifier 10.1109/JEDS.2018.2835818

Diffusive-Probabilistic Model for Inter-Pixel Crosstalk in HgCdTe Focal Plane Arrays

MARCO VALLONE [1], MICHELE GOANO [1,2], FRANCESCO BERTAZZI [1,2], GIOVANNI GHIONE [1], STEFAN HANNA [3], DETLEF EICH [3], AND HEINRICH FIGGEMEIER [3]

1 Dipartimento di Elettronica e Telecomunicazioni, Politecnico di Torino, 10129 Turin, Italy
2 IEIIT-CNR, 10129 Turin, Italy
3 AIM Infrarot-Module GmbH, D-74072 Heilbronn, Germany

CORRESPONDING AUTHOR: M. VALLONE (e-mail: marco.vallone@polito.it)

ABSTRACT A closed-form probabilistic model for inter-pixel crosstalk in planar HgCdTe focal plane arrays is presented, providing simple expressions of crosstalk as function of device parameters like the pixel pitch, the absorber thickness, and the extension of the carrier depleted region. The method is effective in particular for performing parameter sensitivity studies on inter-pixel crosstalk, as an alternative to large-scale numerical simulations. The model is validated against three-dimensional combined optical and electrical numerical simulations, considering realistic, non-monochromatic illumination.

INDEX TERMS Focal plane arrays, crosstalk, infrared detectors, non-monochromatic simulations.

I. INTRODUCTION

Advanced infrared (IR) imaging systems conceived for civilian and military applications employ as key components large format focal plane arrays (FPAs), whose spatial resolution greatly depends on the density of pixels per unit area [1]–[8]. Since FPAs spatially sample the imaged scene, a critical reference value is the minimum useful FPA pixel pitch P for diffraction-limited optical systems. In [8]–[10] the minimum pitch is estimated as $P \approx 2\,\mu$m for the mid-wavelength IR band (MWIR, wavelength $\lambda \in [3, 5]\,\mu$m) and $P \approx 5\,\mu$m for the long-wavelength IR band (LWIR, $\lambda \in [8, 14]\,\mu$m).

When such technologically challenging target values for P are considered, it is important to keep under control inter-pixel crosstalk [5], which includes a number of separate phenomena that may be occurring in the detector or read-out integrated circuit (ROIC) simultaneously. In the present work, with *inter-pixel crosstalk* we mean the electrical response of a FPA pixel when an IR beam illuminates another pixel of the array, excluding any contribution from the ROIC.

HgCdTe is one of the most versatile materials for detector applications over the entire IR spectrum [6], and among other solutions, mesa-type structures [11]–[14], or microlenses [15], [16] may be helpful to minimize some of the possible sources of inter-pixel crosstalk. In mesa-type structures, the deep trenches between pixels help in preventing *diffusive* inter-pixel crosstalk, a deleterious effect due to carriers that, photogenerated in the quasi-neutral region of a pixel, diffuse to neighboring ones [5], [17], [18]. However, large format HgCdTe-based FPAs are often fabricated as planar structures, where two-dimensional (2D) arrays of photodiodes are obtained by ion implantation on a p- or n-doped HgCdTe substrate, giving them n-on-p or p-on-n polarity [19]–[21]. Planar FPAs do not require etching, a source of surface damage and passivation issues in mesa trenches [20]. However, planar arrays may be prone to diffusive inter-pixel crosstalk, that limits the benefits of pitch reduction because of the typically large diffusion length of minority carriers. For n-on-p HgCdTe FPAs, the electron diffusion length L_n is in the order of tens of micrometers [18] for high quality LWIR detectors at operating temperature $T \approx 77$ K.

Inter-pixel crosstalk has been extensively investigated for several semiconductor materials both experimentally (see [11], [16], [22], [23] for III-V-based and Si-based detectors, [13], [24], [25] for HgCdTe detectors) and through numerical simulations [11], [16], [18], [22], [26]–[38]. Concerning the diffusive inter-pixel crosstalk, Kamins and Fong [27] and later Dhar *et al.* [29] developed a probabilistic model, showing that the electric

field E could be instrumental in reducing considerably the inter-pixel diffusive crosstalk, thus increasing the image sharpness. In these early works, the effect of E on the carrier collection probability was evaluated considering P between 20 and 60 μm, much larger than the present state of the art, and a uniform field E in the whole pixel. In addition, these authors avoided to calculate explicitly the profile of excess minority carriers $n'(z) = n(z) - n_d(z)$ from the continuity equation under illumination, where n and n_d are respectively the electron density under illumination and in dark, and assumed instead *a priori* $n'(z) \propto \exp(-\alpha z)$, where α is the absorption coefficient of the semiconductor material, z is the epitaxial growth direction, and $z = 0$ defines the plane of the illuminated face of the detector. However, the expected inter-pixel crosstalk explicitly depends on the $n'(z)$ profile, that in turn is substantially affected both by the illumination conditions, and by the adopted electrical and optical boundary conditions (BC).

In recent years, the approach of carrier-depleting the HgCdTe absorber layer, using either high bias voltage or appropriate compositional and doping profiles [39]–[42], has received attention as a method of reducing the dark current, especially for higher operating temperature (HOT) detector systems. The model described in the present work shows that carrier depletion may be helpful also in reducing considerably the inter-pixel diffusive crosstalk, as already argued by [27] and [29] in different types of detectors. We proceed in two steps: after selecting as our case study a planar HgCdTe LWIR FPA inspired by the literature and the adopted illumination conditions (Section II), first we define and simulate the quantum efficiency (QE) and the inter-pixel crosstalk by means of combined optical and electrical three-dimensional (3D) numerical simulations (Section III). Then, in Section IV we present a diffusive-probabilistic model, validated against the results of Section III, that evaluates the inter-pixel diffusive crosstalk from the pixel geometry and the n' profile calculated according to a diffusion model and appropriate boundary conditions. The obtained closed-form expressions allow to express the diffusive inter-pixel crosstalk as a function of the FPA design parameters (pixel pitch, epitaxial layer thickness, extension of the carrier-depletion region). Finally, the main results are summarized in Section V.

II. THE CASE STUDY

We consider as reference structure the LWIR 5×5 HgCdTe pixel miniarray shown in Fig. 1, where the pixels have *n*-on-*p* polarity [18], [37]. It consists of a $Hg_{0.774}Cd_{0.226}Te$ planar layer with uniform composition and thickness t along the vertical growth direction, *p*-doped with an acceptor density $N_A = 5 \times 10^{15}\,\mathrm{cm}^{-3}$. Each pixel is identified by a $P \times P \times t$ cell, where $P = 5\,\mu$m and t ranges between 2 and 12 μm. The array has a 100% fill factor without any trench between pixels, hence the pitch P is equal to the pixel width. The geometry and doping profiles were generated making use of the Synopsys TCAD Sentaurus 3D numerical simulator [43]: the photodiode junction is defined by simulating an ion implantation, yielding an error-function-shaped donor density N_D ranging from $10^{17}\,\mathrm{cm}^{-3}$ just below the bias contact to $5 \times 10^{14}\,\mathrm{cm}^{-3}$ at the junction, whose type is also known as $n^+ - \nu - p$, often employed in similar devices [18], [19], [44], [45] in order to obtain very low dark current by reducing Auger generation. In this way a low-doped LWIR detector with cutoff wavelength $\lambda_c = 10\,\mu$m at $T = 77$ K is obtained. The substrate is not included in the computational box, and all sides are left uncoated. Ground contacts are connected to the lateral sides of the *p*-doped FPA region, and the bias contacts are connected to the *n*-doped FPA regions through square metallic layers $4\mu\mathrm{m} \times 4\mu\mathrm{m}$ wide, partly extending over a 0.3 μm thick CdTe passivation layer that covers the upper face of the FPA.

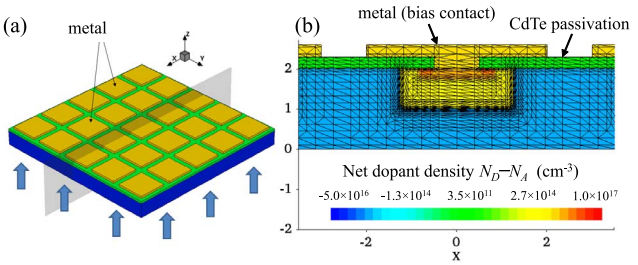

FIGURE 1. (a) The back-illuminated three-dimensional 5 × 5 HgCdTe miniarray under investigation (radiation is represented by vertical arrows). (b) A portion of the two-dimensional cut along the vertical plane shown in panel (a), reporting the net dopant density profile $N_D - N_A$, with the mesh and details of CdTe passivation and metallization.

We consider two illumination conditions: *a*) narrow Gaussian beam illumination, and *b*) plane wave uniform illumination. In the first case, we simulate an optical system that focuses a normally incident, quite narrow, Gaussian beam onto the back face of the detector. The beam, with power flux $\Phi(r) = \Phi_0 \exp(-2r^2/w_0^2)$, is centered on the miniarray central pixel (CP) and focused on the illuminated face. Φ_0 is the optical power flux along the beam axis, r is the radial distance from the beam axis and w_0 is the beam waist radius, for which we chose $w_0 = 3.4\,\mu$m. It must be noticed that $\Phi(r)$ never goes to zero, hence the beam tail partially illuminates also the CP neighboring pixels. In the second case, we illuminate the back face of the miniarray with plane waves having a propagation vector normal to the illuminated face and power flux Φ_0.

Non-monochromatic IR blackbody radiation was considered, with blackbody temperature $T_B = 300$ K and 800 K, limiting the spectral window to wavelengths $\lambda \in [5, 10]\,\mu$m. In all the treated cases, we set $\Phi_0 = 1\,\mathrm{mW\ cm}^{-2}$ when integrated in the considered λ-interval.

III. NUMERICAL SIMULATION OF QUANTUM EFFICIENCY AND INTER-PIXEL CROSSTALK

The HgCdTe optical, electrical properties, Auger and radiative recombination processes are described through the models reported in [18, Table I]. Shockley-Read-Hall (SRH)

recombination is modeled as in [19], [46], and [47] considering a lifetime around 2 μs. Fermi-Dirac statistics and incomplete dopant ionization are taken into account, with activation energies for HgCdTe alloys estimated according to [48] and [49]. In all simulations, we set a lattice temperature $T = 77$ K and we apply a reverse bias $V_{\text{bias}} = 0.1$V simultaneously to all the 5×5 pixels.

The photocurrent $I_{ph,k}$ collected by the bias contact of the k-th pixel strongly depends on the illuminating conditions and allows to define the related (external) quantum efficiency QE_k as

$$\text{QE}_k = \frac{I_{ph,k}}{qN_{ph,k}}, \tag{1}$$

where $N_{ph,k}$ is the photon flux impinging the illuminated face and q is the elementary charge. Relevant figures of merit are the quantum efficiency of the CP and of its nearest neighboring pixels (NNs), respectively indicated as QE_{CP} and QE_{NNs}, and defined according to (1).

In Section III-A we summarize the numerical models employed to attain $I_{ph,k}$ for all the considered illumination conditions and optical source spectra. Then, in Sections III-B and C, QE_{CP} and the inter-pixel crosstalk obtained by numerical simulations are evaluated and discussed, providing a motivation to develop a simplified, analytical model in order to achieve a better understanding of the obtained results.

A. OPTICAL AND ELECTRICAL SOLUTIONS

Considering a monochromatic radiation with wavelength λ, the detector photoresponse depends on the optical generation rate G_{opt}. For brevity of notation, the dependence on wavelength and spatial coordinates are always omitted, unless required for clarity. Maxwell's equations for the electric and magnetic fields $\vec{E}$ and $\vec{H}$ are discretized and solved on a cubic grid known as the Yee grid [50] (the optical mesh has $\approx 3.7 \times 10^5$ points when $t = 2\,\mu$m) according to a Finite Difference Time Domain (FDTD) approach [51], employing a commercial code [52] and treating contact metallizations as Perfect Electric Conductors (PEC) [51]. The computational box includes air layers located above and below the miniarray, and the optical BC along the upper and lower sides of the box are absorbing (in FDTD, this is obtained with convolutional perfectly matching layers [53]), while periodic optical BCs are applied along the lateral sides of the computational box. In the FDTD model, the material properties are represented by the λ-dependent electric permittivity and conductivity ϵ and σ, calculated from the material complex refractive index, see [18], [44] for details. The absorbed photon density A_{opt} (number of absorbed photons per unit volume and time) can be evaluated as the divergence of the time-averaged Poynting vector $\langle\vec{S}\rangle$ [54], [55]

$$A_{\text{opt}} = -\frac{\vec{\nabla}\cdot\langle\vec{S}\rangle}{h\nu} = \frac{1}{2h\nu}\sigma|\vec{E}|^2, \tag{2}$$

where $h\nu$ is the photon energy. The optical generation rate distribution G_{opt} into the pixel due to interband optical absorption is given by $G_{\text{opt}} = \eta A_{\text{opt}}$, where the quantum yield η, defined as the fraction of absorbed photons which are converted to photogenerated electron-hole pairs, was assumed to be unitary.

The spectrum of non-monochromatic optical source is sampled at $N = 16$ equally spaced frequency points ν_i corresponding to wavelengths $\lambda_i \in [5, 10]\,\mu$m, and the resulting photogeneration rate distribution $\overline{G}$ is evaluated from the monochromatic rates $G_{\text{opt}}(\nu_i)$ as

$$\overline{G} = \frac{1}{N}\sum_{i=1}^{N} G_{\text{opt}}(\nu_i)\; w_i(T_{\text{B}}) \tag{3}$$

where the spectral weight coefficients $w_i(T_{\text{B}})$ depend on Planck's law [56] distribution $B(\nu, T_{\text{B}})$:

$$w_i(T_{\text{B}}) = \frac{B(\nu_i, T_{\text{B}})}{\sum_{n=1}^{N} B(\nu_n, T_{\text{B}})}. \tag{4}$$

The resulting rate distribution $\overline{G}$ depends on T_{B} (that is omitted for brevity throughout the present work) and is employed in the electrical simulation of the miniarray.

The electrical simulation is performed discretizing the array in Fig. 1 into $\approx 7 \times 10^5$ elements (when $t = 2\,\mu$m) with a meshing tool which generates a denser grid in regions where gradients of current density, electric field, free charge density and material composition are present. The simulator solves the electrical problem within the drift-diffusion (DD) framework, taking into account the composition, doping, and temperature dependence of the HgCdTe alloy. Electric contacts are treated as Ohmic with zero resistance, where charge neutrality and equilibrium are assumed. Ideal Neumann BCs are applied to the outer boundaries of the array, and the DD equations are solved by the Finite Boxes (FB) method. The optical generation rate $\overline{G}$ due to a given illumination is a source term in the continuity equations for the electron and hole current densities, solved self-consistently with Poisson's equation [47], [57] to obtain the photocurrent $I_{ph,k}$ [18].

B. QUANTUM EFFICIENCY

Uniform illumination is the usual choice employed to characterize the overall detector QE, strongly dependent on the radiation wavelength. Thanks to the uniformity of the illumination ($N_{ph,k}$ is the same for all the pixels) and to the symmetry of the FPA, the net current density between pixels in the xy-plane is approximately zero, and the simulated photocurrent $I_{ph,k}$ is the same for all the pixels. Consequently, also the values of QE_k are approximately the same for all k's, and the averaged value $\text{QE}_0 = \langle\text{QE}_k\rangle$ well represents, as usually intended for this figure of merit, the capability of the detector to convert an optical signal into an electrical one. We excluded from the average the outer ring of the 5×5 miniarray, to avoid small discrepancies due to border effects.

On the contrary, a narrow *Gaussian beam* centered on the central pixel is not a standard choice to obtain a QE. In this case QE_{CP}, defined according to (1) for $k = \text{CP}$, leads

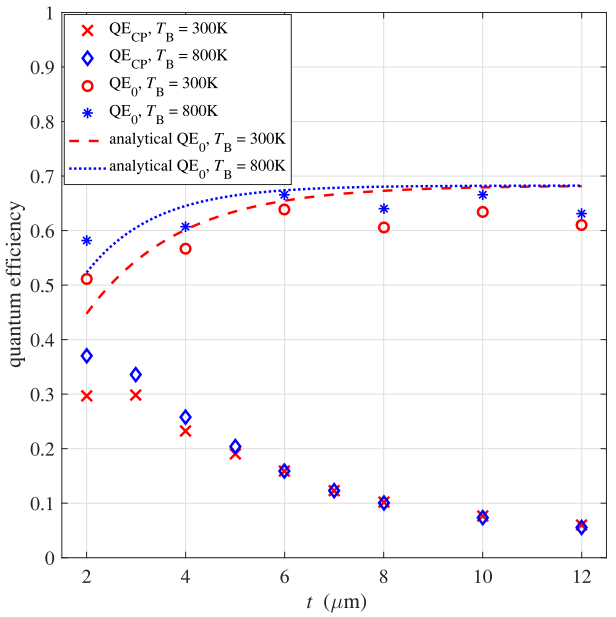

FIGURE 2. Numerical simulation of the quantum efficiency for Gaussian beam illumination QE_{CP} (crosses and diamonds), and for uniform illumination QE_0 (circles and stars), for blackbody sources with $T_B = 300$ K and 800 K. The analytic form of QE_0 (uniform illumination) according to (5) is also reported (dashed and dotted lines).

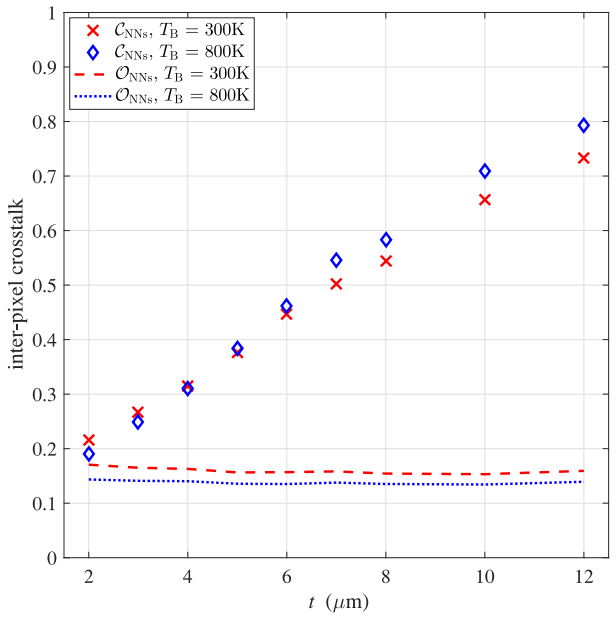

FIGURE 3. Numerical simulation of the *total* (symbols) and *optical* (dashed and dotted lines) inter-pixel crosstalk, for Gaussian beam illumination with $T_B = 300$ K and 800 K blackbody spectra.

to highly informative results. In Fig. 2 we plot the numerically simulated values of QE_{CP} and QE_0 as functions of t. Their opposite behaviors are particularly striking, since QE_0 monotonically increases with t, whereas QE_{CP} monotonically decreases, as if a thicker absorber worked against the detector QE. Thus, a more detailed discussion is required to explain this behavior.

The simulated QE_0 approximately follows the behavior described by the analytic expression of the quantum efficiency for a planar detector when illuminated by plane waves [58, Ch. 6] in absence of interference effects [18]

$$QE_0(t) \approx (1-R)\left(1-e^{-\overline{\alpha}t}\right), \tag{5}$$

valid for $t \ll L_n$ and $\overline{\alpha}L_n \gg 1$ (see Fig. 2, dashed and dotted lines). Here $R = (\overline{n}-1)^2/(\overline{n}+1)^2$ is the mean air/HgCdTE reflection coefficient [59], and $\overline{\alpha}$ and $\overline{n}$ are the mean values of the $Hg_{0.774}Cd_{0.226}Te$ absorption coefficient and refractive index, averaged on the interval $\lambda_i \in [5,\ 10]\,\mu$m as done for G_{opt} in (3). In the present case one has $\overline{\alpha} = 0.5331\,\mu\text{m}^{-1}$ and $R = 0.3158$ for $T_B = 300$ K, $\overline{\alpha} = 0.7269\,\mu\text{m}^{-1}$ and $R = 0.3192$ for $T_B = 800$ K, and $L_n \approx 140\,\mu$m at $T = 77$ K. It may be noticed that plane wave illumination makes cavity effects particularly prominent, visible in Fig. 2 as oscillations of numerically simulated QE_0. They are due to internal back-reflections at the metallization, addressed and studied on very similar devices in [18] and [44], under monochromatic illumination. Simple expressions like (5) of course cannot reproduce this feature.

Concerning the behavior of $QE_{CP}(t)$, rather than a measure of the detector quantum efficiency, it is related to the inter-pixel crosstalk. In the present work we will address in particular two among its possible contributions, the *diffusive* and the *optical* crosstalk, whose definitions are given in Section III-C.

C. INTER-PIXEL CROSSTALK

Electrical simulations allow to define a useful figure of merit, *i.e.,* the ratio $\mathscr{C}_i$ between the photocurrent collected by the electrical contact of the i-th pixel and of the CP,

$$\mathscr{C}_i = \frac{I_{ph,\,i}}{I_{ph,\,\text{CP}}}, \tag{6}$$

that can be regarded as a possible definition of the *total* inter-pixel crosstalk (excluding ROIC). Considering in particular the NNs, $\mathscr{C}_{NNs}$ has contributions originating both from *electrical* and from *optical* effects, since it depends *a*) on carriers photogenerated in the CP diffusing to the neighboring ones (*diffusive* crosstalk), and *b*) on carriers directly photogenerated in the NNs by the illuminating Gaussian beam tail [18] (*optical* crosstalk). The latter can be defined as the ratio between carriers photogenerated in one of the NNs (with volume V_{NNs}) and those photogenerated in the CP (with volume V_{CP})

$$\mathscr{O}_{NNs} = \frac{\int_{V_{NNs}} \overline{G}(x,y,z)\,dx\,dy\,dz}{\int_{V_{CP}} \overline{G}(x,y,z)\,dx\,dy\,dz}. \tag{7}$$

In Fig. 3 we plot the numerically simulated *total* and *optical* inter-pixel crosstalks $\mathscr{C}_{NNs}$ and $\mathscr{O}_{NNs}$. The former is monotonically increasing with t, just the way QE_{CP} is decreasing in Fig. 2. The latter is in practice independent of t, therefore we may argue that the diffusive contribution

to $\mathscr{C}_{\mathrm{NNs}}$ is the component responsible of its increase with t. In fact, we expect that *a*) for small values of t the crosstalk is mostly *optical* (in Fig. 3 $\mathscr{C}_{\mathrm{NNs}}$ tends to $\mathscr{O}_{\mathrm{NNs}}$ for small t), and *b*) *diffusive* crosstalk monotonically increases with t, since carrier diffusion is expected to be increasingly effective as t increases.

The question now is whether we can write $\mathscr{C}_{\mathrm{NNs}} = \mathscr{O}_{\mathrm{NNs}} + \mathscr{D}_{\mathrm{NNs}}$ as an exact equality, where $\mathscr{D}_{\mathrm{NNs}}$ is the *diffusive* crosstalk. The answer is that we can accept this claim only as an approximate equality, provided the beam is narrow enough (smaller than the pixel pitch). In fact, the photocurrent $I_{ph,\mathrm{NNs}}$ detected in one of the NNs is the sum of a *diffusive* contribution $I_{\mathrm{diff,NNs}}$ coming from carriers photogenerated in the CP and diffused to the NNs, and an *optical* contribution $I_{\mathrm{tail,NNs}}$ coming from carriers really photogenerated in the NNs themselves by the beam tail, proportional to $\int_{V_{\mathrm{NNs}}} \overline{G}(x, y, z)\, dx\, dy\, dz$, hence proportional to $\mathscr{O}_{\mathrm{NNs}}$. Therefore, defining *diffusive* crosstalk as the ratio

$$\mathscr{D}_{\mathrm{NNs}} = \frac{I_{\mathrm{diff,NNs}}}{I_{ph,\mathrm{CP}}}, \tag{8}$$

since it is $I_{\mathrm{diff,NNs}} = I_{ph,\mathrm{NNs}} - I_{\mathrm{tail,NNs}}$, at least as a first approximation we get from (6) and (7)

$$\mathscr{D}_{\mathrm{NNs}} = \mathscr{C}_{\mathrm{NNs}} - \frac{I_{\mathrm{tail,NNs}}}{I_{ph,\mathrm{CP}}} \approx \mathscr{C}_{\mathrm{NNs}} - \mathscr{O}_{\mathrm{NNs}}, \tag{9}$$

having exploited for the approximate equality the proportionality between the photocurrent and the integral of $\overline{G}$ over the detector volume appearing in the definition of $\mathscr{O}_{\mathrm{NNs}}$. Eq. (9) neglects a small (provided the beam is narrow) contribution to $I_{ph,\mathrm{CP}}$ originating from carriers photogenerated in the NNs (because of the beam tail) that diffuse to the CP. We will use this definition of $\mathscr{D}_{\mathrm{NNs}}$ in Section IV, where a simple model will be shown to reproduce also quantitatively the simulation results shown in Fig. 2 and Fig. 3.

IV. DIFFUSIVE-PROBABILISTIC MODEL FOR INTER-PIXEL CROSSTALK

2D and 3D simulation results were found to show good agreement in dark and under illumination [60], provided the photodetector is symmetric. Exploiting this property, we consider a 2D cut of the miniarray, further simplified as in Fig. 4, consisting of a quasi-neutral region where the magnitude of the electric field E is zero, and a fully depleted $d \times a$ region where E is high (in numerical simulations, we find $E \approx 10^{-4}$ V/cm and $E \approx 10^{3}$ V/cm in quasi-neutral and space charge regions, respectively, for reverse bias $V_{\mathrm{bias}} = 0.1$V). On top of each depleted region, bias contacts remove the photogenerated carriers, considered as immediately swept out as soon as they reach the depleted regions.

With reference to Fig. 4, assuming all the carriers as photogenerated only along the vertical z-axis, and following an approach similar to [27] and [29], on average only carriers diffusing within the angle θ reach the CP depleted region and are collected. With similar considerations, only carriers

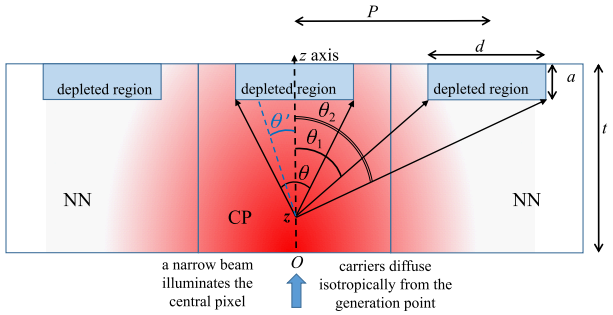

FIGURE 4. 2D scheme of the simplified pixels array for the diffusive-probabilistic model in the *xz* plane. Carriers photogenerated in *z* diffuse isotropically. Only the fraction of them within θ can reach the CP depleted region and is assumed to contribute to $I_{ph,\mathrm{CP}}$. The fraction of carriers within $\theta_2 - \theta_1$, instead, contributes to $I_{ph,\mathrm{NNs}}$, giving origin to the diffusive inter-pixel crosstalk.

diffusing within the angle $|\theta_2 - \theta_1|$ can reach one of the NNs, contributing to NNs crosstalk. If we define $F(z, \theta') = \exp(-|x|/L_n) = \exp(-z|\tan(\theta')|/L_n)$, the probability to find in (x, z) a carrier photogenerated along the z-axis is approximately proportional to $F(z, \theta')\, \rho(z)$ [27], [29], where $\rho(z)$, still to be determined, depends both on diffusion and absorption coefficient. Furthermore, if $N_0(z) = \int_{-\pi/2}^{\pi/2} F(z, \theta') d\theta'$, the probability that a carrier is collected by the CP contact or by one of the NNs is given respectively by

$$W_{\mathrm{CP}}(t, z) = N_0^{-1}(z) \int_{-\theta/2}^{\theta/2} F(z, \theta') d\theta'$$
$$W_{\mathrm{NNs}}(t, z) = N_0^{-1}(z) \int_{\theta_1}^{\theta_2} F(z, \theta') d\theta'. \tag{10}$$

Since it is $L_n \gg (d, P)$, we can consider a Taylor's expansion for F in $(|x|/L_n)$, obtaining the approximate expressions $W_{\mathrm{CP}}(t, z) = \theta/\pi + O(d/L_n)$ and $W_{\mathrm{NNs}}(t, z) = |\theta_2 - \theta_1|/\pi + O((d/2 + P)/L_n)$, that explicitly read

$$W_{\mathrm{CP}}(t, z) \approx \frac{2}{\pi} \arctan\left(\frac{d/2}{t - a - z}\right)$$
$$W_{\mathrm{NNs}}(t, z) \approx \frac{1}{\pi} \left| \arctan\left(\frac{P + d/2}{t - a - z}\right) - \arctan\left(\frac{P - d/2}{t - a - z}\right) \right|. \tag{11}$$

For the sake of simplicity, we employed the approximate expressions (11) throughout the present work, accepting an error on the resulting crosstalk that we verified to be around 2%, consistent with the first order correction to the Taylor's expansion for F. However, we stress that for smaller values of L_n, it may be more advisable to employ (10) instead. Hence, the CP quantum efficiency reads

$$\widetilde{\mathrm{QE}}_{\mathrm{CP}}(t) = \mathrm{QE}_0(t) \int_0^{t-a} W_{\mathrm{CP}}(t, z) \rho(z) dz, \tag{12}$$

where $\rho(z) = n'(z) / \int_0^{t-a} n'(\zeta) d\zeta$. Within the present model, the *diffusive* crosstalk $\widetilde{\mathscr{D}}_{\mathrm{NNs}}$ can be defined as

$$\widetilde{\mathscr{D}}_{\mathrm{NNs}} = \frac{\int_0^{t-a} W_{\mathrm{NNs}}(t, z) \rho(z) dz}{\int_0^{t-a} W_{\mathrm{CP}}(t, z) \rho(z) dz}, \tag{13}$$

and both $\widetilde{\mathrm{QE}}_{\mathrm{CP}}$ and $\widetilde{\mathscr{D}}_{\mathrm{NNs}}$ depend on $n'(z)$ through $\rho(z)$, that we determined in an approximate way, considering a simple one-dimensional (1D) model of diffusion along z, neglecting any optical interference effect [18], [44]. In short, in the p-doped quasi-neutral region of the absorber the photogenerated carriers are assumed to diffuse, but not to drift, since $E \approx 0$. The solution of the diffusion equation of minority carriers in stationary regime

$$D_n \frac{d^2 n'}{dz^2} = \frac{n'}{\tau_n} - G(z) \tag{14}$$

yields the density profile $n'(z)$. Here $D_n = L_n^2/\tau_n$ is the electron diffusion coefficient, τ_n its lifetime, and $G(z)$ the carrier photogeneration rate per unit volume and time. The IR radiation enters the absorber at $z = 0$ with wavevector along z and is progressively absorbed following Beer's absorption law [47, Sec. 1.6.2]. In absence of internal reflections and interference effects, the $G(z)$ profile is given by $G(z) = G_0 \exp(-\overline{\alpha} z)$, where G_0 it the photogeneration rate at $z = 0$.

Boundary conditions are not a trivial problem. The literature on CMOS detectors and solar cells usually adopts

$$v_{rec} n'(0) = D_n \left.\frac{dn'}{dz}\right|_{z=0}, \quad n'(t-a) = 0, \tag{15}$$

where v_{rec} is the carriers recombination velocity on the ground contact, usually located in $z = 0$ (see [26] and references therein, or the recent review [23]). The second BC in (15) means that, for $z > t-a$, the electric field prevents any accumulation of electrons by quickly sweeping them across the depletion region. Concerning the detector under exam, the second BC still holds, but the first does not, since in the real 3D device the ground contact is not located in $z = 0$, but laterally, therefore a more realistic couple of BCs for this device are $n'(0) = n'_0$ and $n'(t-a) = 0$, where the first BC is determined by the photogeneration, that sets the excess carrier density at $z = 0$ as $n'_0 = G_0 \tau_n$. Imposing such BCs, the solution of the inhomogeneous differential equation (14) follows from standard methods and is given by

$$n'(z) = n'_0 \frac{\overline{\alpha}^2 L_n^2}{\overline{\alpha}^2 L_n^2 - 1} \left[\frac{\sinh\left(\frac{t-a-z}{L_n}\right)}{\sinh\left(\frac{t-a}{L_n}\right)} + \frac{e^{-\overline{\alpha} z}}{\overline{\alpha}^2 L_n^2} \times \left(\frac{e^{-\overline{\alpha}(t-a-z)} \sinh\left(\frac{z}{L_n}\right)}{\sinh\left(\frac{t-a}{L_n}\right)} - 1 \right) \right]. \tag{16}$$

As a check, when $\overline{\alpha} L_n \gg 1$ as in the present case, (16) reduces to the known, textbook form [47, Sec. 1.8.2]

$$n'(z) = n'_0 \frac{\sinh\left(\frac{t-a-z}{L_n}\right)}{\sinh\left(\frac{t-a}{L_n}\right)}. \tag{17}$$

It is interesting to compare the CP QE and the *diffusive* crosstalk obtained by the numerical simulations of Section III and by the present diffusive-probabilistic model, assuming

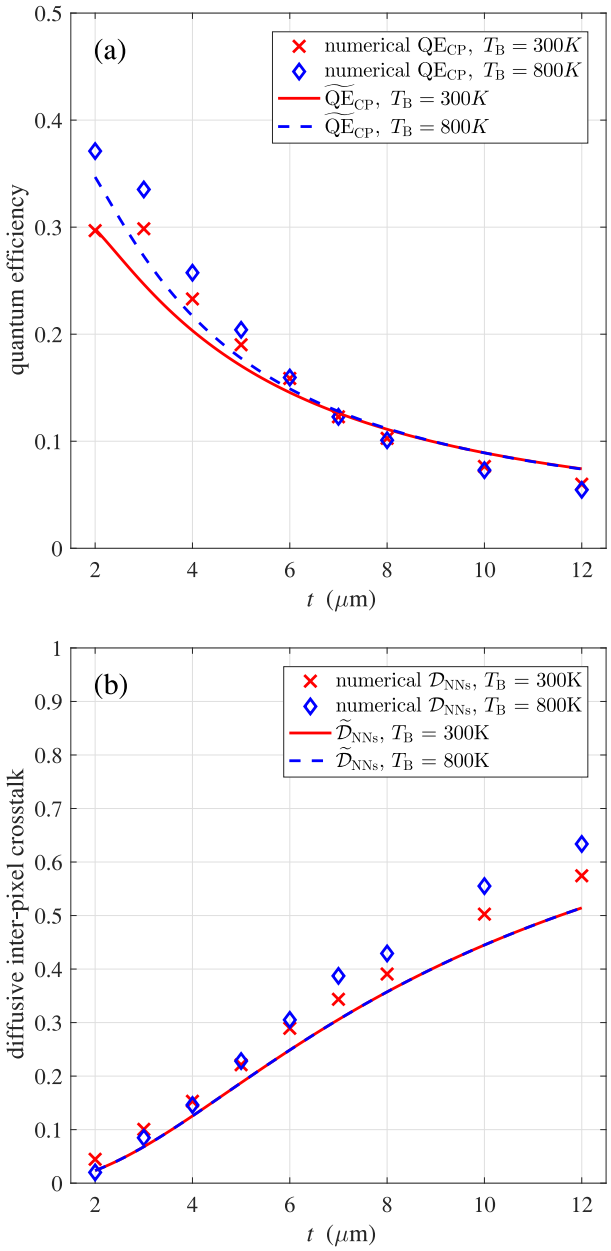

FIGURE 5. (a) Plot of $\widetilde{\mathrm{QE}}_{\mathrm{CP}}$, according to (12) (solid and dashed lines), with the numerical values of $\mathrm{QE}_{\mathrm{CP}}$ already shown in Fig. 2 (symbols). (b) Plot of the inter-pixel crosstalk $\widetilde{\mathscr{D}}_{\mathrm{NNs}}$ according to (13), with the numerical values of $\mathscr{D}_{\mathrm{NNs}}$ according to (9) (symbols).

$d = 2\,\mu$m and $a = 1.1\,\mu$m, consistent with the geometry of the depleted region shown in Fig. 1(b). In Fig. 5(a) we compare $\mathrm{QE}_{\mathrm{CP}}$ with $\widetilde{\mathrm{QE}}_{\mathrm{CP}}$, and in Fig. 5(b) $\mathscr{D}_{\mathrm{NNs}}$ with $\widetilde{\mathscr{D}}_{\mathrm{NNs}}$. Within the adopted approximations, the agreement may be considered satisfactory, and the use of (13) turns out to be a fast way to calculate the expected diffusive inter-pixel crosstalk in planar structures with simple, symmetric geometry, provided pixels can be considered composed by a quasi-neutral and a high E (space charge) region, a common occurrence in HgCdTe photodiodes [39], [41], [61], [62],

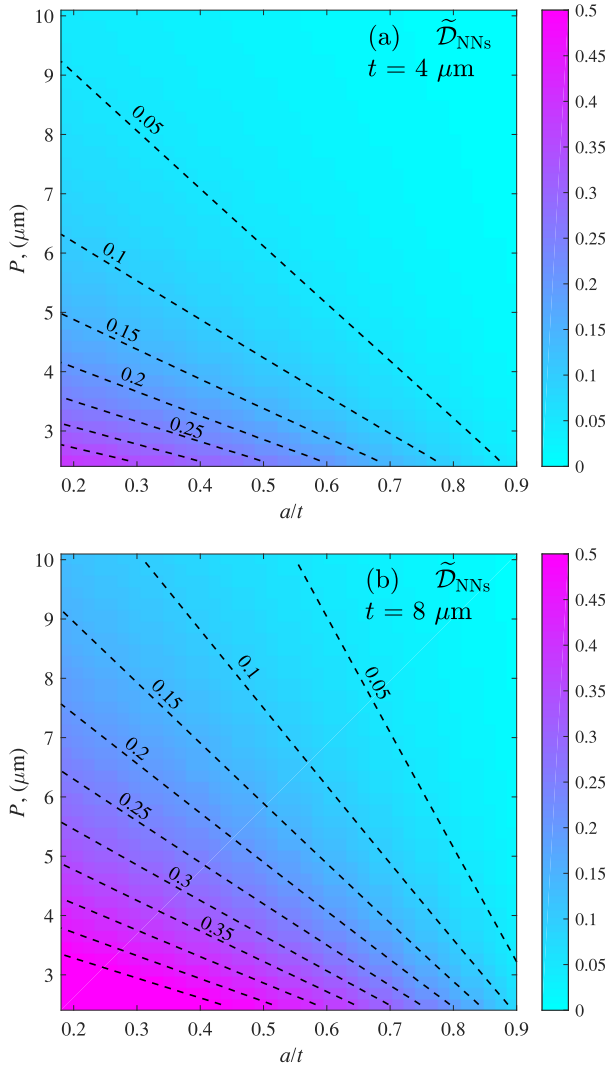

FIGURE 6. Example of use of the present model: color maps of $\widetilde{\mathcal{D}}_{\mathrm{NNs}}$, as function of pixel pitch P and ratio a/t, for $t = 4\ \mu$m (a) and for $t = 8\ \mu$m (b).

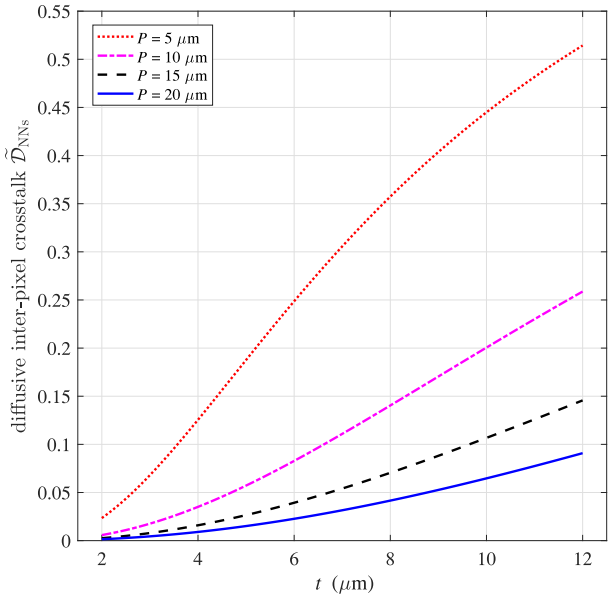

FIGURE 7. The inter-pixel crosstalk $\widetilde{\mathcal{D}}_{\mathrm{NNs}}(t)$ for several values of pixel pitch P, showing the progressive increase of diffusive inter-pixel crosstalk when P is reduced towards the target value, $P \approx 5\ \mu$m (other parameters: $d = 2\ \mu$m, $a = 1.1\ \mu$m, $\bar{\alpha}$ for a $T_{\mathrm{B}} = 300$ K blackbody illumination).

but also in nBn photodetectors [6] and in CCD and CMOS image sensors [63].

Differences between $\widetilde{\mathcal{D}}_{\mathrm{NNs}}$ and $\mathcal{D}_{\mathrm{NNs}}$, more evident for the highest values of t, come from the adoption of a simplified 1D model for $n'(z)$, and from the effects of internal reflections, included in $\mathcal{D}_{\mathrm{NNs}}$, but neglected in $n'(z)$ and $\widetilde{\mathcal{D}}_{\mathrm{NNs}}$. Despite these limitations, Fig. 5 shows that the present diffusive-probabilistic model can be considered accurate enough for identifying design rules in order to keep diffusive crosstalk under control. As an example of use, in Fig. 6 we show 2D maps of $\widetilde{\mathcal{D}}_{\mathrm{NNs}}$ as functions of the pixel pitch P and the fraction of absorber depleted from carriers a/t, having considered two different values of absorber thickness t and a $T_{\mathrm{B}} = 300$ K blackbody illumination. We observe that, if the diffusive crosstalk has to be lower than 10%, a planar FPA with pixel pitch $P = 5\ \mu$m requires $a/t > 0.4$ if $t = 4\ \mu$m. Instead, if $t = 8\ \mu$m, the required fraction of depleted absorber increases to $a/t > 0.7$, supporting the efforts of several research teams to achieve full-depletion in the absorber [41], [64]–[66], in addition to their primary goal of reducing the dark current in HOT detectors. In fact, the pitch reduction in planar FPAs towards the target values referred to in Section I entails higher amount of inter-pixel crosstalk, as shown in Fig. 7 where we plot $\widetilde{\mathcal{D}}_{\mathrm{NNs}}$ as function of t for several values of pixel pitch P.

V. CONCLUSION

The diffusive and optical inter-pixel crosstalk in HgCdTe IR planar FPA detectors have been investigated. 3D numerical simulations, performed by commercial codes that solve the optical problem with a full-wave FDTD method and the electrical problem with a finite-box method within the drift-diffusion approximation, have allowed to calculate the inter-pixel crosstalk under realistic, non-monochromatic illumination, assessing in particular the effects of absorber thickness and carrier depletion. Exploiting its spatial symmetry [60], we considered a 2D section of the miniarray, developing an approximate, closed-form model, aimed at a better understanding of the effects of diffusion on crosstalk. The challenging solution of the resulting 2D diffusion problem has been avoided, developing instead a probabilistic description complementing a much more tractable 1D diffusion model. In this way, it has been possible to obtain compact expressions for diffusive crosstalk, suitable to develop design rules to keep diffusive crosstalk under control, acting on pixel pitch, absorber thickness, extension and depth of the absorber depleted region. The closed-form model has been validated against the results of 3D numerical simulations. The applicability of the present model is not limited to HgCdTe, provided the electric field into each

pixel allows to define a low-field and a high-field (depleted) region.

REFERENCES

[1] M. A. Kinch, "Fundamental physics of infrared detector materials," *J. Electron. Mater.*, vol. 29, no. 6, pp. 809–817, 2000.

[2] W. E. Tennant, D. Lee, M. Zandian, E. Piquette, and M. Carmody, "MBE HgCdTe technology: A very general solution to IR detection, described by 'rule 07,' a very convenient heuristic," *J. Electron. Mater.*, vol. 37, no. 9, pp. 1406–1410, 2008.

[3] A. Rogalski, J. Antoszewski, and L. Faraone, "Third-generation infrared photodetector arrays," *J. Appl. Phys.*, vol. 105, no. 9, 2009, Art. no. 091101.

[4] C. A. Keasler and E. Bellotti, "A numerical study of broadband absorbers for visible to infrared detectors," *Appl. Phys. Lett.*, vol. 99, no. 9, 2011, Art. no. 091109.

[5] J. Schuster *et al.*, "Numerical simulation of third-generation HgCdTe detector pixel arrays," *IEEE J. Sel. Topics Quantum Electron.*, vol. 19, no. 5, pp. 1–15, Sep./Oct. 2013.

[6] P. Martyniuk, J. Antoszewski, M. Martyniuk, L. Faraone, and A. Rogalski, "New concepts in infrared photodetector designs," *Appl. Phys. Rev.*, vol. 1, no. 4, 2014, Art. no. 041102.

[7] O. Gravrand *et al.*, "HgCdTe detectors for space and science imaging: General issues and latest achievements," *J. Electron. Mater.*, vol. 45, no. 9, pp. 4532–4541, 2016.

[8] A. Rogalski, P. Martyniuk, and M. Kopytko, "Challenges of small-pixel infrared detectors: A review," *Rep. Progr. Phys.*, vol. 79, no. 4, 2016, Art. no. 046501.

[9] G. C. Holst and R. G. Driggers, "Small detectors in infrared system design," *Opt. Eng.*, vol. 51, no. 9, 2012, Art. no. 096401.

[10] R. G. Driggers, R. Vollmerhausen, J. P. Reynolds, J. Fanning, and G. C. Holst, "Infrared detector size: How low should you go?" *Opt. Eng.*, vol. 51, no. 6, 2012, Art. no. 063202.

[11] A. Nedelcu, H. Gwénaëlle, D. Adrien, M. Sylvain, and B. de l'Isle Nadia, "Low pitch LWIR QWIPs: Performance level and image quality," *Infrared Phys. Technol.*, vol. 70, pp. 129–133, May 2015.

[12] R. K. McEwen, D. Jeckells, S. Bains, and H. Weller, "Developments in reduced pixel geometries with MOVPE grown MCT arrays," in *Proc. SPIE Infrared Techol. Appl. XLI*, vol. 9451. Baltimore, MD, USA, 2015, Art. no. 94512D.

[13] S. B. Rafol *et al.*, "Low frequency $1/f$ noise on QWIPs, nBn, and superlattice focal plane array," *Infrared Phys. Technol.*, vol. 84, pp. 50–57, Aug. 2017.

[14] H. Figgemeier *et al.*, "State-of-the-art MCT photodiodes for cutting-edge sensor applications by AIM," in *Proc. SPIE Infrared Techol. Appl. XLIII*, vol. 10177. Anaheim, CA, USA, 2017, Art. no. 101771K.

[15] O. Akın and H.-V. Demir, "Mid-wave infrared metasurface microlensed focal plane array for optical crosstalk suppression," *Opt. Exp.*, vol. 23, no. 21, pp. 27020–27027, 2015.

[16] O. Akın and H.-V. Demir, "High-efficiency low-crosstalk dielectric metasurfaces of mid-wave infrared focal plane arrays," *Appl. Phys. Lett.*, vol. 110, no. 14, 2017, Art. no. 143106.

[17] B. Pinkie and E. Bellotti, "Numerical simulation of spatial and spectral crosstalk in two-color MWIR/LWIR HgCdTe infrared detector arrays," *J. Electron. Mater.*, vol. 42, no. 11, pp. 3080–3089, 2013.

[18] M. Vallone *et al.*, "Simulation of small-pitch HgCdTe photodetectors," *J. Electron. Mater.*, vol. 46, no. 9, pp. 5458–5470, 2017.

[19] M. Vallone *et al.*, "Numerical modeling of SRH and tunneling mechanisms in high-operating-temperature MWIR HgCdTe photodetectors," *J. Electron. Mater.*, vol. 44, no. 9, pp. 3056–3063, 2015.

[20] S. Hanna *et al.*, "MCT-based LWIR and VLWIR 2D focal plane detector arrays for low dark current applications at AIM," *J. Electron. Mater.*, vol. 45, no. 9, pp. 4542–4551, 2016.

[21] D. Eich *et al.*, "Progress of MCT detector technology at AIM towards smaller pitch and lower dark current," *J. Electron. Mater.*, vol. 46, no. 9, pp. 5448–5457, 2017.

[22] M. S. Ünlü and S. Strite, "Resonant cavity enhanced photonic devices," *J. Appl. Phys.*, vol. 78, no. 2, pp. 607–639, 1995.

[23] B. Blanco-Filgueira, P. L. Martínez, and J. B. R. Aranda, "A review of CMOS photodiode modeling and the role of the lateral photoresponse," *IEEE Trans. Electron Devices*, vol. 63, no. 1, pp. 16–25, Jan. 2016.

[24] T. J. Sanders, E. L. Caraway, G. T. Hess, G. W. Newsome, and T. Fischer, "Modeling and test of pixel cross-talk in HgCdTe focal plane arrays," in *Proc. SPIE Infrared Technol. Appl. XXVII*, vol. 4369. Orlando, FL, USA, 2001, pp. 458–466.

[25] A. V. Vishnyakov, V. A. Stuchinsky, D. V. Brunev, A. V. Zverev, and S. A. Dvoretsky, "Determination of charge-carrier diffusion length in the photosensing layer of HgCdTe n-on-p photovoltaic infrared focal plane array detectors," *Appl. Phys. Lett.*, vol. 104, no. 9, 2014, Art. no. 092112.

[26] M. H. Crowell and E. F. Labuda, "The silicon diode array camera tube," *Bell Syst. Tech. J.*, vol. 48, no. 5, pp. 1481–1528, May/Jun. 1969.

[27] T. I. Kamins and G. T. Fong, "Photosensing arrays with improved spatial resolution," *IEEE Trans. Electron Devices*, vol. ED-25, no. 2, pp. 154–159, Feb. 1978.

[28] R. M. Fastow and A. Strum, "Monte Carlo simulations of the cross talk in InSb matrices," in *Proc. SPIE Infrared Technol. Appl. XLIII*, vol. 2274. San Diego, CA, USA, 1994, pp. 136–146.

[29] V. Dhar, R. K. Bhan, and R. Ashokan, "Effect of built-in electric field on crosstalk in focal plane arrays using HgCdTe epilayers," *Infrared Phys. Technol.*, vol. 39, no. 6, pp. 353–367, 1998.

[30] D. D'Orsogna, S. P. Tobin, and E. Bellotti, "Numerical analysis of a very long-wavelength HgCdTe pixel array for infrared detection," *J. Electron. Mater.*, vol. 37, no. 9, pp. 1349–1355, 2008.

[31] C. A. Keasler, M. Moresco, D. D'Orsogna, P. Lamarre, and E. Bellotti, "3D numerical analysis of As-diffused HgCdTe planar pixel arrays," in *Proc. SPIE Detectors Imag. Devices Infrared Focal Plane Single Photon*, vol. 7780. San Diego, CA, USA, 2010, Art. no. 77800J.

[32] G. Soehnel and A. Tanbakuchi, "Simulation and experimental characterization of the point spread function, pixel saturation, and blooming of a mercury cadmium telluride focal plane array," *Appl. Opt.*, vol. 51, no. 33, pp. 7987–7993, 2012.

[33] B. Pinkie and E. Bellotti, "Large-scale numerical simulation of reduced-pitch HgCdTe infrared detector arrays," in *Proc. SPIE Infrared Technol. Appl. XXXIX*, vol. 8704. Baltimore, MD, USA, 2013, Art. no. 87042S.

[34] E. Bellotti, J. Schuster, B. Pinkie, and F. Bertazzi, "Multiscale modeling of photon detectors from the infrared to the ultraviolet," in *Proc. SPIE Infrared Sensors Devices Appl. III*, vol. 8868. San Diego, CA, USA, 2013, Art. no. 88680R.

[35] J. Berthoz *et al.*, "Modeling and characterization of MTF and spectral response at small pitch on mercury cadmium telluride," *J. Electron. Mater.*, vol. 44, no. 9, pp. 3157–3162, 2015.

[36] B. Pinkie, A. R. Wichman, and E. Bellotti, "Modulation transfer function consequences of planar dense array geometries in infrared focal plane arrays," *J. Electron. Mater.*, vol. 44, no. 9, pp. 2981–2989, 2015.

[37] M. Vallone *et al.*, "Broadband 3D optical modeling of HgCdTe infrared focal plane arrays," in *Proc. 17th Int. Conf. Numer. Simulat. Optoelectron. Devices (NUSOD)*, Copenhagen, Denmark, Jul. 2017, pp. 205–206.

[38] T. Zhang *et al.*, "MTF measurement and analysis of linear array HgCdTe infrared detectors," *Infrared Phys. Technol.*, vol. 88, pp. 123–127, Jan. 2018.

[39] W. Lei, J. Antoszewski, and L. Faraone, "Progress, challenges, and opportunities for HgCdTe infrared materials and detectors," *Appl. Phys. Rev.*, vol. 2, no. 4, 2015, Art. no. 041303.

[40] P. Martyniuk *et al.*, "Dark current suppression in HOT LWIR HgCdTe heterostructures operating in non-equilibrium mode," *J. Infrared Millim. Waves*, vol. 34, no. 4, pp. 385–390, 2015.

[41] J. Schuster, R. DeWames, and P. S. Wijewarnasurya, "Dark currents in a fully-depleted LWIR HgCdTe *P*-on-*n* heterojunction: Analytical and numerical simulations," *J. Electron. Mater.*, vol. 46, no. 11, pp. 6295–6305, 2017.

[42] J. Schuster, W. E. Tennant, E. Bellotti, and P. S. Wijewarnasuriya, "Analysis of the Auger recombination rate in $P^+N^-n^-N^-N$ HgCdTe detectors for HOT applications," in *Proc. SPIE Infrared Technol. Appl. XLII*, vol. 9819. Baltimore, MD, USA, 2016, Art. no. 98191F.

[43] *Sentaurus Device User Guide. Version M-2017.09*, Synopsys, Inc., Mountain View, CA, USA, Sep. 2017.

[44] M. Vallone *et al.*, "Comparing FDTD and ray-tracing models in numerical simulation of HgCdTe LWIR photodetectors," *J. Electron. Mater.*, vol. 45, no. 9, pp. 4524–4531, 2016.

[45] K.-M. Mahlein *et al.*, "Next generation IR sensor technology for space applications at AIM," in *Proc. SPIE*, vol. 7106. Cardiff, U.K., Oct. 2008, pp. 1–10.
[46] W. Shockley and W. T. Read, "Statistics of the recombinations of holes and electrons," *Phys. Rev.*, vol. 87, no. 5, pp. 835–842, 1952.
[47] S. M. Sze and K. K. Ng, *Physics of Semiconductor Devices*, 3rd ed. Hoboken, NJ, USA: Wiley, 2007.
[48] A. Rogalski, *Infrared Detectors*, 2nd ed. Boca Raton, FL, USA: CRC Press, 2011.
[49] P. Capper and J. Garland, Eds., *Mercury Cadmium Telluride. Growth, Properties and Applications*. Chichester, U.K.: Wiley, 2011.
[50] K. Yee, "Numerical solution of initial boundary value problems involving Maxwell's equations in isotropic media," *IEEE Trans. Antennas Propag.*, vol. AP-14, no. 3, pp. 302–307, May 1966.
[51] D. Vasileska, S. M. Goodnick, and G. Klimeck, *Computational Electronics. Semiclassical and Quantum Device Modeling and Simulation*. Boca Raton, FL, USA: CRC Press, 2010.
[52] *RSoft FullWAVE User Guide, v2017.03*, Synopsys, Inc., Ossining, NY, USA, 2017.
[53] J.-P. Berenger, "A perfectly matched layer for the absorption of electromagnetic waves," *J. Comput. Phys.*, vol. 114, no. 2, pp. 185–200, 1994.
[54] M. Born and E. Wolf, *Principles of Optics. Electromagnetic Theory of Propagation, Interference and Diffraction of Light*, 7th ed. Cambridge, U.K.: Cambridge Univ. Press, 1999.
[55] C. A. Keasler and E. Bellotti, "Three-dimensional electromagnetic and electrical simulation of HgCdTe pixel arrays," *J. Electron. Mater.*, vol. 40, no. 8, pp. 1795–1801, 2011.
[56] C. Kittel and H. Kroemer, *Thermal Physics*. San Francisco, CA, USA: Freeman, 1980.
[57] S. Selberherr, *Analysis and Simulation of Semiconductor Devices*. Vienna, Austria: Springer-Verlag, 1984.
[58] J. Chu and A. Sher, *Device Physics of Narrow Gap Semiconductors*. New York, NY, USA: Springer-Verlag, 2010.
[59] J. Piprek, *Semiconductor Optoelectronic Devices: Introduction to Physics and Simulation*. San Diego, CA, USA: Academic, 2003.
[60] M. Vallone *et al.*, "Modeling photocurrent spectra of single-color and dual-band HgCdTe photodetectors: Is 3D simulation unavoidable?" *J. Electron. Mater.*, vol. 43, no. 8, pp. 3070–3076, 2014.
[61] A. Jóźwikowska *et al.*, "Generation-recombination effects on dark currents in CdTe-passivated midwave infrared HgCdTe photodiodes," *J. Appl. Phys.*, vol. 98, no. 1, 2005, Art. no. 014504.
[62] A. M. Itsuno, J. D. Phillips, and S. Velicu, "Predicted performance improvement of Auger-suppressed HgCdTe photodiodes and *p-n* heterojunction detectors," *IEEE Trans. Electron Devices*, vol. 58, no. 2, pp. 501–507, Feb. 2011.
[63] I. Djité *et al.*, "Theoretical models of modulation transfer function, quantum efficiency, and crosstalk for CCD and CMOS image sensors," *IEEE Trans. Electron Devices*, vol. 59, no. 3, pp. 729–737, Mar. 2012.
[64] P. K. Saxena, "Modeling and simulation of HgCdTe based p^+-n^--n^+ LWIR photodetector," *Infrared Phys. Technol.*, vol. 54, no. 1, pp. 25–33, 2011.
[65] W. E. Tennant *et al.*, "Small-pitch HgCdTe photodetectors," *J. Electron. Mater.*, vol. 43, no. 8, pp. 3041–3046, 2014.
[66] D. Lee *et al.*, "High-operating temperature HgCdTe: A vision for the near future," *J. Electron. Mater.*, vol. 45, no. 9, pp. 4587–4595, 2016.

MARCO VALLONE received the Laurea degree in physics from the Università di Torino, Italy, and the Ph.D. degree in electronic devices from the Politecnico di Torino, Turin, Italy, in 1985 and 2016, respectively. From 1985 to 1999, he was with Telecom Italia, working in a testing and design facility for telecommunications and optoelectronics. From 1999 to 2008, he was with Avago Technologies (a spin-off of Agilent Technologies), working in design and modeling of optoelectronic devices. From 2008 to 2016, he was a Fellow with the Politecnico di Torino, where he has been a Post-Doctoral Fellow since 2016. His current research activity is focused on the simulation of optoelectronic devices based on narrow- and wide-bandgap semiconductor materials, and on the description of inter- and intra-band quantum scattering processes in the Green's function formalism.

MICHELE GOANO (M'98) received the Laurea and Ph.D. degrees in electronic engineering from the Politecnico di Torino, Turin, Italy, in 1989 and 1993, respectively. In 1994, he was a Post-Doctoral Fellow with the Département de Génie Physique, École Polytechnique de Montréal, Montréal, QC, Canada. He joined the faculty of the Politecnico di Torino in 1995. He has been a Visiting Scholar with the School of Electrical and Computer Engineering, Georgia Institute of Technology, Atlanta, GA, USA, with the Department of Information Technology and Media, Mid-Sweden University, Sundsvall, Sweden, and the Department of Electrical and Computer Engineering, Boston University, Boston, MA, USA. His current research activity is focused on the simulation of optoelectronic devices based on narrow- and wide-bandgap semiconductor materials.

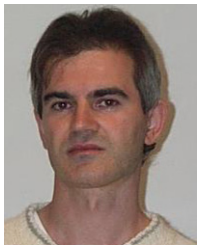

FRANCESCO BERTAZZI received the Laurea and Ph.D. degrees in electronics engineering from the Politecnico di Torino, Turin, Italy, in 2000 and 2003, respectively. He was a Visiting Scholar with the Department of Electrical and Computer Engineering, Boston University, Boston, MA, USA. Since 2008, he has been a Professor with the Dipartimento di Elettronica, Politecnico di Torino. His Ph.D. studies were focused on electromagnetic modeling of traveling-wave structures for optoelectronic applications and nonlinear physics-based noise analysis of RF and microwave devices. His research activities with Boston University included material-theory-based modeling of band structures, vibrational properties, and carrier scattering rates, essential for the study of the complex electronic, transport, and optical properties of novel wide-gap semiconductors, in particular III-nitrides and II-VI oxide semiconductors. His present research activity is focused on density matrix and nonequilibrium Green's function modeling of carrier transport and recombination processes in optoelectronic devices (HgCdTe infrared photodetectors, InGaN light-emitting diodes, and VCSELs).

GIOVANNI GHIONE received the graduation degree (*cum laude*) in electronic engineering from the Politecnico di Torino, Turin, Italy, in 1981. He has been a Full Professor in electronics since 1990. His research activity has been mainly concerned with high-frequency electronics and optoelectronics. He has contributed to the physics-based modeling of compound semiconductor devices, with particular interest in the numerical noise modeling in the small- and large-signal regimes, in the thermal modeling of devices and integrated circuits, and in the modeling of widegap semiconductors devices and materials. He has also done research in the field of microwave electronics, with contributions in the modeling of passive elements, in particular coplanar components, and in the design of power MMICs. Since 1985, he has been actively engaged in research on optoelectronic devices, with application to the modeling and design of near and far-IR photodetectors, electrooptic and electroabsorption modulators, and GAN-based LEDs. He has authored or co-authored over 300 research papers on the above subjects and five books. He has been a member of the QPC subcommitee of IEDM from 1997 to 1998 and from 2006 to 2007 and the Chair in 2008; from 2009 to 2010, he was the EU Arrangement Co-Chair of IEDM. From 2010 to 2015, he was the Chair of the EDS Committee on Compound Semiconductor Devices and Circuits. He has been the Chair of the GAAS2003 conference and the Subcommittee Chair in several SCs of the European Microwave Week. Since 2016, he has been the Editor-in-Chief of the IEEE TRANSACTIONS ON ELECTRON DEVICES. He was the President of the Library System of Politecnico from 1997 to 2007. From 2007 to 2015, he was the Head of the Department of Electronics and Telecommunications of Politecnico di Torino.

STEFAN HANNA received the M.Sc. degree in physics and the Ph.D. degree from Universität Bayreuth, Germany, in 2002 and 2008, respectively. He has been with AIM Infrarot-Module GmbH since 2007, working from 2007 to 2010 in the electro-optical characterization of SWIR, LWIR, and VLWIR detectors for space applications within the space projects group of the AIM Division Sensors. From 2008 to 2015, he was a Project Manager of various TRP research and development studies with the European Space Agency, a Manager with the System Design of the AIM Division Space Program, and from 2014 to 2017, he works in sensor development within the AIM Division Sensors. Since 2018, he has been a Manager with Photodiode Array Development, Division Sensors, AIM.

DETLEF EICH received the M.Sc. degree in physics and the Ph.D. degree from Universität Würzburg, Germany, in 1996 and 2000, respectively. He has been with AIM Infrarot-Module GmbH, Heilbronn, since 2000. From 2000 to 2009, he was a Development Staff Member with the Development of FPA Technology for CMT IR Photodetectors, Division Sensors, AIM. From 2009 to 2012, he was a Manager with the Development FPA-Technology, Division Sensors. From 2012 to 2014, he was a Manager with Operations Projects, Division Sensors. Since 2014, he has been a Manager with Development, Division Sensors.

HEINRICH FIGGEMEIER received the M.Sc. degree in physics from Universität Paderborn, Germany, in 1989. From 1989 to 1995, he was with AEG, Heilbronn, as a Development Staff Member with the Development of Liquid Phase Epitaxy for CMT IR Photodetectors. In 1996, he joined AIM Infrarot-Module GmbH, where he is a Manager of Product Planning and FPA-Technology, Division Sensors from 1996 to 2009. From 2009 to 2013, he was a Manager with Division Sensors, AIM, and since 2014, he has been the Head of Division Sensors, AIM.